JOURNAL OF MATERIALS SCIENCE **34** (1999) 2609–2620

Thermal evolution crystal structure and cation valence of Mn in substituted Ba-β-Al_2O_3 prepared via coprecipitation in aqueous medium

G. GROPPI*, M. BELLOTTO‡, C. CRISTIANI, P. FORZATTI
Dipartimento di Chimica Industriale e Ingegneria Chimica "G. Natta", Politecnico di Milano, Piazza Leonardo da Vinci 32, 20133 Milano, Italy
E-mail: gianpiero.groppi@polimi.it

PL. VILLA
Dipartimento di Chimica, Ingegneria Chimica e Materiali, Università de L' Aquila, 67040 Monteluco di Roio (AQ), Italy

$BaMn_xAl_{12-x}O_{19-\alpha}$ combustion catalysts with $x = 0.5$, 1.0, 2.0, 3.0 have been prepared via coprecipitation in aqueous medium. Thermal evolution from 380 up to 1670 K has been followed by XRD and surface area measurements. The crystal structure of the final material and the dominant oxidation state of Mn in the different crystallographic sites, have been investigated by means of XANES spectroscopy and Rietveld refinements of diffraction powder data sets collected in proximity and far from the Mn*K* absorption edge. It was found that, except for the highest Mn content ($x = 3$), monophasic samples are obtained upon calcination at 1470 K. For the whole compositional range the Ba-β_l-Al_2O_3 structure is obtained. A formation mechanism involving Ba ion diffusion within the γ-Al_2O_3 spinel blocks, similar to that observed for Mn-free samples, is active also in this case. However, the presence of Mn ions favours the formation of the Ba-β_l-Al_2O_3 that occurs at lower temperatures. At low Mn loading (up to $x = 1$), Mn preferentially enters the tetrahedral Al(2) sites of the Ba-β_l-Al_2O_3 as Mn^{2+}. At higher loading, Mn preferentially enters the octahedral Al(1) sites as Mn^{3+}. A charge compensation mechanism, involving the occupancy of Ba sites in the mirror planes, operates to balance the substitution of Al^{3+} with Mn^{2+}. The presence of Mn ions also affects the morphological properties of the final material. © *1999 Kluwer Academic Publishers*

1. Introduction

Ba-hexaaluminates are considered suitable materials for gas turbine applications in view of their high thermal stability [1, 2]. They retain surface areas of 10–15 m^2/g upon calcination at 1570 K. This property has been related to the peculiar layered structure of the material that consists of alternative stacking along the *c* axis of spinel blocks containing Al^{3+} ions, and mirror planes in which large divalent and/or trivalent cations (e.g. Ba, Ca, Sr, La) are located. Depending on the composition and the defectivity of the mirror plane, β-Al_2O_3 or magnetoplumbite-like structures are obtained. Measurements of anisotropic diffusion of oxide ions showed a reduced ion diffusion rate along the *c* axis [3]. This results in a limited ability for rearrangement of the stacking sequence that causes a preferential exposure of mirror planes at the surface and prevents coalescence of the crystallite along the *c* axis [4]. As a result, typical platelike crystallites, characterised by a strong anisotropy, form in these materials. For unsubstituted Ba-β-Al_2O_3 the existence of two different phases, β_I and β_{II}, with different Ba contents have been demonstrated. In Ba-poor samples the β_I phase with composition $Ba_{0.75}Al_{11}O_{17.25}$ forms; this corresponds to the ideal Na-β-Al_2O_3 ($NaAl_{11}O_{17}$) in which, to maintain electroneutrality with respect to substitution of monovalent sodium with divalent barium ions, a quarter of the Ba^{2+} in the mirror plane (Beevers-Ross sites) is replaced by O^{2-} (Reidinger defects) [5]. In Ba-rich samples the β_{II} phase with composition $Ba_{1.167}Al_{10.667}O_{17.167}$ is formed with Ba ions located in both spinel blocks and mirror planes [6]. For intermediate compositions, i.e. $BaAl_{12}O_{19}$, the final structure originates from the intergrowth of β_I and β_{II} domains [4].

Combustion activity can be obtained by introducing transition metal ions into the structure [2]. This does not modify the physical properties of the material, and Mn-substituted samples exhibit high thermal stability with surface areas of 15–20 m^2/g being retained following calcination at 1670 K.

* Author to whom all correspondence should be addressed.
‡ *Present address:* CTG, Rue des Technodes, 78931 Guerville Cedex, France.

Arai and co-workers studied Mn-substituted materials prepared via alkoxides hydrolysis [7]. They reported that monophasic samples are obtained for $BaMn_xAl_{12-x}O_{19-\alpha}$ up to $x = 2$ and that segregation of $BaAl_2O_4$ occurs upon further Mn addition. Smets and Verlijsdonk [8] observed that incorporation of Mn in Ba-rich samples results in the formation of the β_I phase and in the segregation of $BaAl_2O_4$. They also observed a strong analogy between Mn and Mg-doped Ba-β-Al_2O_3 [8], suggesting that Mn is located in the spinel blocks as Mn^{2+}. Along these lines Electron Paramagnetic Resonance (EPR) studies on single crystals of doped Na-β-Al_2O_3 confirm that Mn is located in the spinel blocks, predominantly as Mn^{2+} in the tetrahedral Al(2) sites [9]. Finally, structural analysis of single crystals of substituted barium hexaaluminate with low Mn content has indicated that, also in this case, Mn is located in the Al(2) sites [3]. Accordingly the incorporation of divalent ions of relatively small size that replace Al^{3+} in tetrahedral Al(2) sites, appears to be a common features of β-Al_2O_3 materials.

All the above studies refer typically to materials doped with small amounts of Mn. However, the study of the effect of large additions of Mn is relevant to the use of these materials as combustion catalysts since it is Mn that is responsible for the catalytic properties. Furthermore, in the papers published so far, neither data on phase composition changes during calcination are reported, nor is the mechanism of formation of the final material discussed.

In a previous paper we reported a characterisation study of Ba-Al-O samples prepared via coprecipitation in aqueous medium of the inorganic precursors of the constituents [10]. In the present work we report on the preparation and characterisation of Ba-Mn-Al-O samples, with Mn/Ba ratios varying from 0.5 to 3, prepared according to the method outlined above. Thermal evolution has been investigated by X-ray diffraction (XRD) and surface area measurement (N_2 adsorption) in order to study phase evolution, morphological properties and formation mechanisms. The crystal structure of the final materials, and the dominant oxidation state of Mn in the different crystallographic sites in substituted Ba-β-Al_2O_3, have been studied by X-ray Absorption Near Edge Structure (XANES) spectroscopy and Rietveld refinements of multiple powder diffraction data sets collected at different wave lengths both in proximity and far from the MnK absorption edge. Synchrotron radiation as well as CuK_α radiation were used for this purpose. The relation between crystal structure and the morphological properties of the final materials are also discussed.

2. Experimental

2.1. Preparation

Four Mn-substituted Ba-β-Al_2O_3 samples with nominal composition $BaMn_xAl_{12-x}O_{19}$ ($x = 0.5, 1, 2$ and 3) were prepared via coprecipitation in aqueous medium, using soluble nitrate salts of the constituents and $(NH_4)_2CO_3$ as precipitating agent. Details of the preparation procedure are reported elsewhere [10, 11].

The precursor materials, obtained upon filtration, washing and overnight drying at 380 K of the cake, were calcined at 470, 770, 970, 1170, 1270, 1370, 1470, 1570 and 1670 K as follows: heating rate 1 K/min; hold at each step 10 h.

Chemical analysis by atomic absorption of the mother liquors and the samples calcined at 1570 K, confirmed that quantitative precipitation was obtained with the measured final compositions corresponding to expectation.

The samples will be quoted in the text with notations referring to the nominal Ba/Mn/Al content and the calcination temperature (e.g. BaMn0.5Al11.5-1270 indicates the sample with expected composition $BaMn_{0.5}Al_{11.5}O_{19}$ calcined at 1270 K).

2.2. Characterisation

The X-ray powder diffraction patterns of the Mn-substituted β-aluminas were measured using Ni-filtered CuK_α radiation (Philips vertical diffractometer PW 1050-70). The data were collected in the angular range 3°–70° 2θ.

Quantitative XRD analyses for the determination of the amount of $BaAl_2O_4$ were performed according to the procedure reported in the literature [12] using the intensity of the (202) $BaAl_2O_4$ reflection calculated by profile fitting. The calibration curve was obtained by preparing mechanical mixtures of γ-Al_2O_3 and $BaAl_2O_4$ in different weight percentages. Surface areas were measured by nitrogen adsorption using a Fison Sorptomatic 1900 series instrument.

EPR spectra of BaMn0.5Al11.5 were collected by a Varian E109 spectrometer.

2.3. XANES experiments and Rietveld structural refinement

For structural analysis, the X-ray powder diffraction patterns of all the Mn-substituted β-aluminas calcined at 1570 K were measured using CuK_α radiation and a pyrolitic graphite diffracted beam monochromator (Philips vertical diffractometer PW 1050-70). The data were collected in the angular range 5°–120° 2θ.

Synthetic Mn_3O_4 (Hausmannite) was used as standard to determine the scattering coefficients of Mn^{2+} and Mn^{3+} in a local co-ordination similar to that of the investigated samples. The X-ray absorption of all the $BaMn_xAl_{12-x}O_{19}$ samples, along with that of the reference, were first measured to calibrate the energy position of the MnK absorption edge. Then, for the BaMn1Al11 and BaMn2Al10 samples, as well as for the reference sample, the X-ray powder patterns were measured at three wavelengths in proximity of the MnK edge, approximately at -20, -50 and -200 eV; the edge position was defined as the maximum of the first derivative peak of the absorption curve. The spectra were collected using synchrotron radiation at line 2.3 of SRS, Daresbury Laboratory. The monochromatic incident beam was obtained using a Si(111) monochromator.

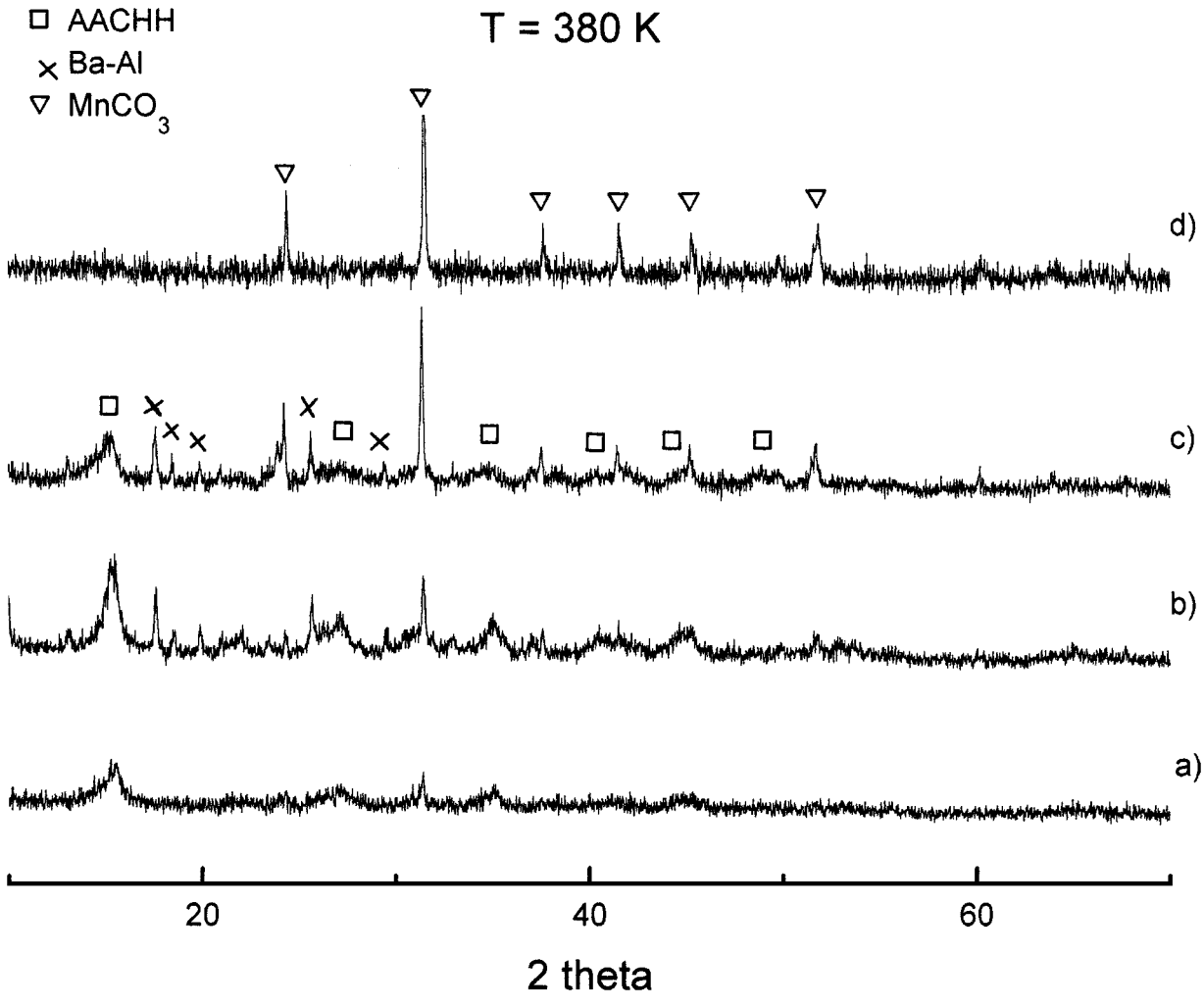

Figure 1 XRD Spectra of samples dried at 380 K: (a) BaMn0.5Al11.5, (b) BaMn1Al11, (c) BaMn2Al10 and (d) BaMn3A19. AACHH (Ammonium, Aluminium Carbonate-Hydroxi-Hydrate) = $(NH_4)_2Al_6(OH)_{14}(CO_3)_3{\cdot}H_2O$; Ba-Al = $Ba_2Al_4(OH)_{16}$, $BaAl_2(CO_3)_2(OH)_4{\cdot}2H_2O$.

The powder diffraction patterns were used in a Rietveld refinement using the GSAS software [13]. Both CuK_α and synchrotron radiation patterns were used in multipattern refinements in cases where several diagrams were measured for the same sample.

3. Results

3.1. Drying (380 K) and calcination at low temperature (770–970 K)

A complex phase composition is observed for all the BaMnxAl$(12-x)$ samples dried at 380 K: their XRD spectra are reported in Fig. 1a–d. Samples with Mn content up to 2 (Fig. 1a–c) consist of a mixture of poorly crystalline $(NH_4)_2Al_6(OH)_{14}(CO_3)_3{\cdot}H_2O$ [14], mixed Ba-Al hydroxides, carbonates and hydroxicarbonates (tentatively $BaAl_2(CO_3)_2(OH)_4{\cdot}2H_2O$ [JCPDS 31-116], $BaAl_4(OH)_{16}$ [JCPDS 24-16]) and $MnCO_3$ Rodhochrosite [JCPDS 7-268], whereas in BaMn3Al9 only $MnCO_3$ is detected (Fig. 1d). Except for the presence of $MnCO_3$, the composition of the dried precursors is similar to that previously reported for unsubstituted Ba-β-Al_2O_3 prepared according to the same procedures [10].

Upon calcination at 770 K, decomposition of the methastable carbonates and hydroxides phases, observed in the dried precursors, occurs. No reflections of crystalline phases are detected in the XRD spectra of BaMnxAl$(12-x)$-770, and only smooth modulations of the base line (at $2\theta \cong 19.4$, 37.6, 39.5, 45.8, 60.9, 67.0) associated with microcrystalline γ-Al_2O_3 [JCPDS 10-425] are barely observed.

On increasing the temperature to 970 K (Fig. 2a–d) the formation of α-Mn_2O_3 is observed in all the samples, in increasing amount with the Mn content. Furthermore, for BaMn3Al9 small amounts of $BaAl_2O_4$ [JCPDS 17-306] are present (Fig. 2d). Moreover, the smooth modulation of the base line, attributable to the features of microcrystalline γ-Al_2O_3 are still present in all the samples.

The dried samples exhibit high surface area values around 100–200 m^2/g, with the higher values corresponding to the lower Mn content (200 and 100 m^2/g for BaMn0.5Al11.5-380 and BaMn3Al9-380 respectively). These values are in line with the observed co-presence of crystalline (i.e. pure and mixed Al and Ba hydroxides, carbonates and hydroxicarbonates and $MnCO_3$) and microcrystalline compounds (i.e. γ-Al_2O_3). Surface area keeps practically constant up to 770 K, whereas upon calcination at 970 K a slight decrease is observed (values are around 90–180 m^2/g) possibly associated with the progressive sintering of the γ-Al_2O_3 matrix.

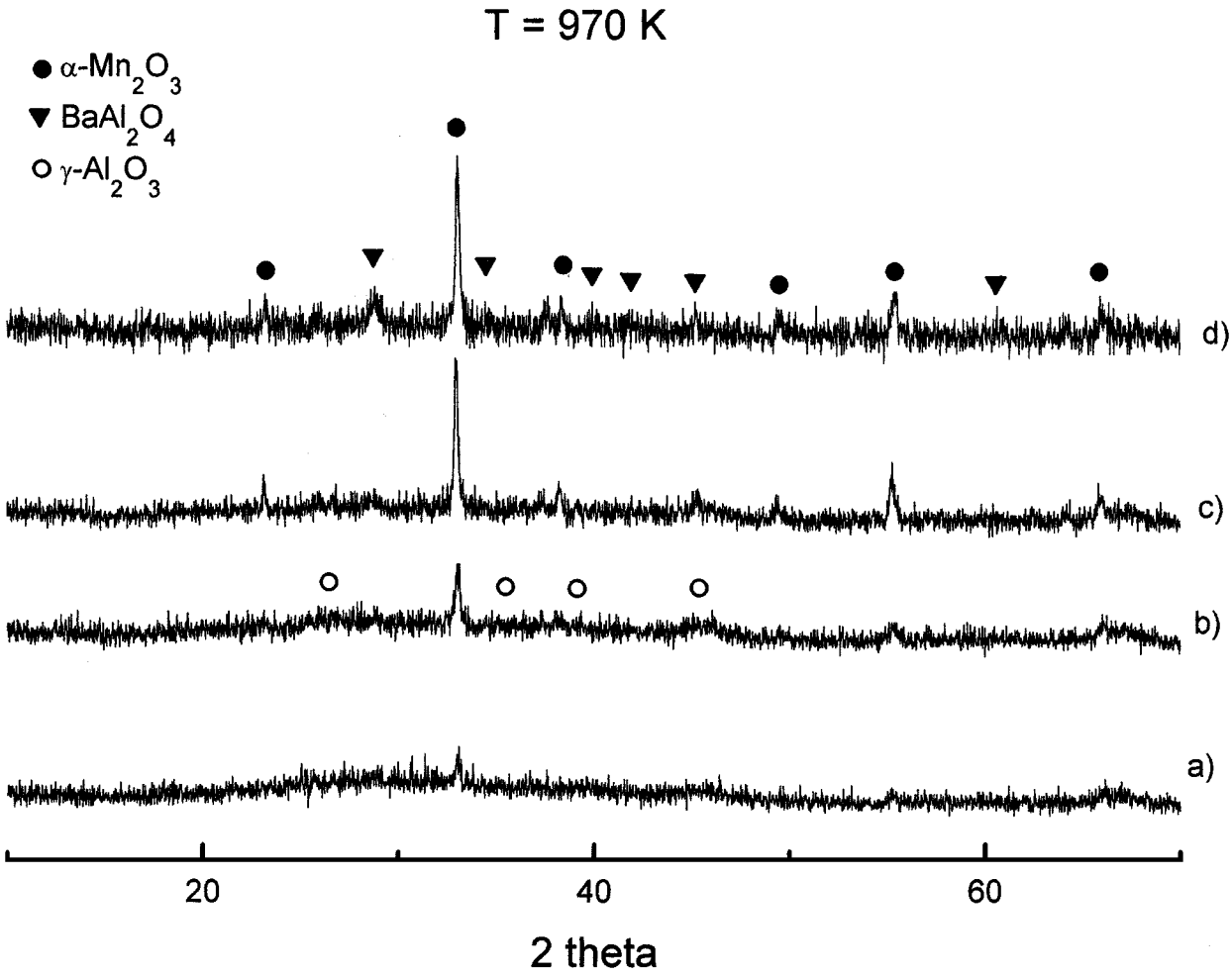

Figure 2 XRD Spectra of samples calcined at 970 K: (a) BaMn0.5Al11.5, (b) BaMn1Al11, (c) BaMn2Al10 and (d) BaMn3Al9.

3.2. Calcination at intermediate (1170–1470 K) and high temperatures (1570–1670 K)

Upon calcination at 1170 K the reflections of crystalline $BaAl_2O_4$ are detected in all the samples, together with those of α-Mn_2O_3 and the modulations of microcrystalline γ-Al_2O_3 (Fig. 3a–d). In BaMn3Al9-1170 (Fig. 3d) small amounts of Ba-β-Al_2O_3 [4, 10] are also present. Accordingly in this sample the formation of the layered alumina phase occurs 200 K below the temperature observed in Mn-free hexaaluminates, i.e. 1370 K [10].

Starting from 1270 K the formation of the Ba-β-Al_2O_3 phase occurs in all samples and is paralleled by the decrease of the reflections of $BaAl_2O_4$ and by the complete disappearance of the α-Mn_2O_3 (Fig. 4a–d). The amount of the Ba-β-Al_2O_3 increases with Mn content: in BaMn2Al10-1270 and BaMn3Al1270 this phase represents the major component, while in the samples with lower Mn loading only minor amounts of the Ba-β-Al_2O_3 form.

In the XRD spectra of the samples calcined at 1370 K the modulations attributed to microcrystalline γ-Al_2O_3 are no longer detected and the Ba-β-Al_2O_3 is always the main phase (Fig. 5a–d). Indeed BaMn1Al11 and BaMn2Al10 are monophasic, whereas only traces of $BaAl_2O_4$ are present in BaMn0.5Al11.5 and BaMn3Al9. Upon calcination at 1470 (Fig. 6a–d), also BaMn0.5Al11.5 becomes monophasic while $BaAl_2O_4$ is still evident in BaMn3Al9. These phase compositions remain stable even upon calcination at 1670 K; accordingly, $BaAl_2O_4$ is always detected in the BaMn3Al9 sample.

The structure and composition of the samples calcined at 1570 K have been accurately investigated by means of Rietveld refinement of the XRD spectra. Details of this analysis will be reported in a following paragraph.

In Fig. 7 the surface areas of the Mn-containing samples, together with those of a reference $BaAl_{12}O_{19}$ sample (BaAl12), are reported as a function of calcination temperature in the range 1170–1670 K. BaMn0.5Al11.5 and BaMn1Al11 exhibit a similar trend with a slight decrease of the surface area between 1170 and 1270 K, followed by a more pronounced decrease between 1270 and 1370 K, that progressively smoothes above 1370 K and reaches a plateau of 15 m^2/g in the range 1470–1670 K. In the BaMn2Al10 sample most of surface area loss occurs between 1170 and 1270 K, whereas, above this temperature, a slight decrease is observed up to 1470 K and again an asymptotic behaviour ($As = 8$–10 m^2/g) is observed up to 1670 K. BaMn3Al9 sinters markedly at temperature lower than 1170 K. The steep decrease of surface area continues up to 1270 K whereas a gradual decrease down to 6 m^2/g is evident upon further

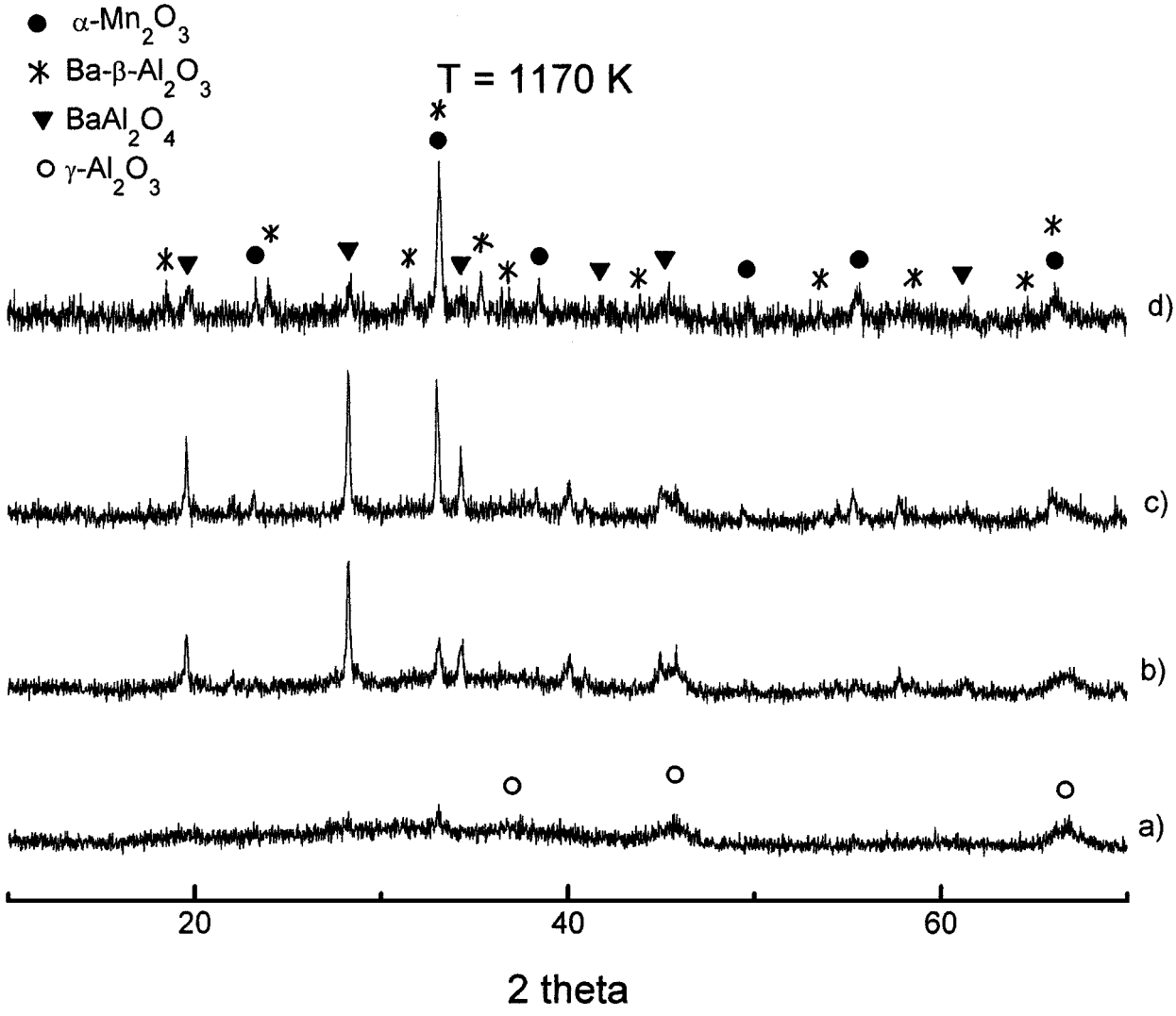

Figure 3 XRD Spectra of samples calcined at 1170 K: (a) BaMn0.5Al11.5, (b) BaMn1Al11, (c) BaMn2Al10 and (d) BaMn3Al9.

calcination at 1570–1670 K. Finally the surface area of the reference BaAl12 sample slowly decreases up to 1370 K and drops markedly between 1370 and 1470 K. Above 1470 K a stable value of 15 m^2/g is observed.

For all the samples the trend of surface area is apparently related to the formation of the final Ba-β-Al_2O_3 phase. Indeed, as described above, this phase at 1170 K is present in minor amounts only in BaMn3Al9; at 1270 K it is the dominant phase in both BaMn3Al9 and BaMn2Al10 whereas it is present only in minor amounts in BaMn0.5Al11.5 and BaMn1Al11. In all the Mn-containing samples monophasic composition is observed at 1370 K except for the presence of small amounts of $BaAl_2O_4$ in BaMn0.5Al11.5 and BaMn3Al9 and finally phase evolution is completed at 1470 K. On the other hand, according to a previous characterisation study [10], in Mn-free BaAl12 samples the formation of Ba-β-Al_2O_3 only starts at 1370 K and is completed at 1570 K.

3.3. Quantitative analysis of $BaAl_2O_4$

As described above, $BaAl_2O_4$ forms in the temperature range 970–1270 K depending on the Mn content. This phase completely disappears between 1370 and 1470 K in BaMn0.5Al11.5, BaMn1Al11 and BaMn2Al10, whereas only small amounts are present in BaMn3Al9 up to 1670 K. To evaluate the extent of the formation of $BaAl_2O_4$, quantitative analysis from XRD powder data has been performed. Results are reported in Fig. 8 together with data of a reference $BaAl_{12}O_{19}$ sample. The following features are observed: (1) in all the samples the relative amount of $BaAl_2O_4$ increases up to a maximum and then progressively decreases; (2) the temperature of the maximum decreases with the Mn content. The highest temperature (1370 K) is observed for the Mn-free BaAl12 sample. BaMn0.5Al11.5 exhibits the maximum at 1270 K, whereas in BaMn1Al11 and BaMn2Al10 the maximum occurs at 1170, finally the lowest temperature (970 K) is observed for BaMn3Al9; (3) the maximum amount of $BaAl_2O_4$ varies with the Mn loading as well: it corresponds to 35–40% (w/w) of the total Ba in BaAl12, ≈25% (w/w) in BaMn1Al11 and BaMn2Al10 and to 8–10% (w/w) in BaMn0.5Al11.5 and BaMn3Al9; (4) residual $BaAl_2O_4$, detected in BaMn3Al9 in the temperature range 1170–1670, is constant and corresponds to ≈5% (w/w) of the total Ba content. As a general trend the maximum amount of Ba segregated as

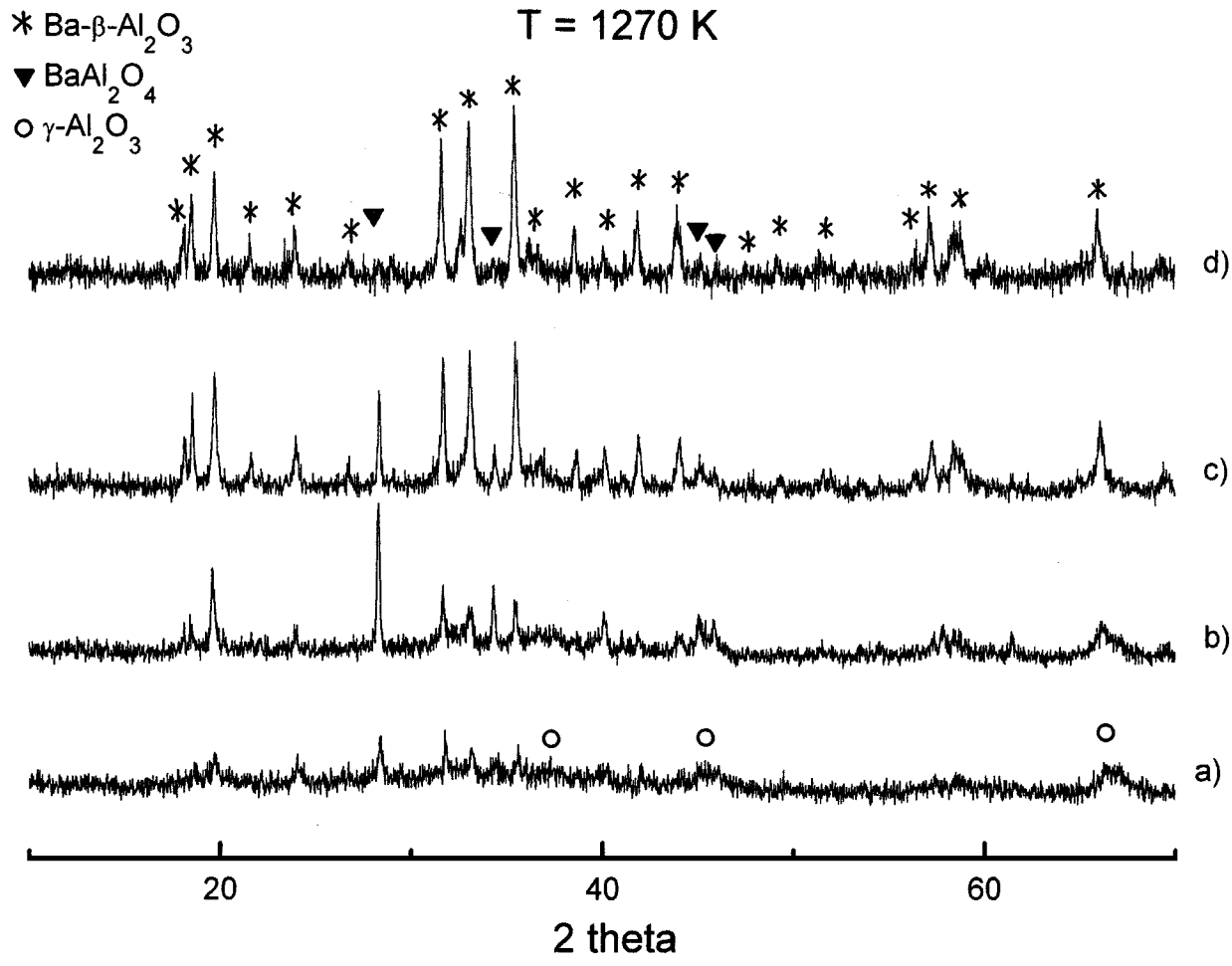

Figure 4 XRD spectra of samples calcined at 1270 K: (a) BaMn0.5Al11.5, (b) BaMn1Al11, (c) BaMn2Al10 and (d) BaMn3Al9.

$BaAl_2O_4$ decreases on increasing the Mn content except for BaMn0.5Al11.5 that shows small amount of $BaAl_2O_4$.

For all the samples from the XRD spectra it is evident that the decrease of $BaAl_2O_4$, parallels the formation of Ba-β-Al_2O_3.

3.4. Structural analysis, allocation and oxidation state of Mn in the structure

The detailed structure of the samples calcined at 1570 K, specifically with respect to Mn location and its valence, was studied by XANES spectroscopy and Rietveld structural refinement.

The Mn XANES diagrams measured over all Mn-substituted Ba-β-Al_2O_3 samples and over the Mn_3O_4 reference sample are shown in Fig. 9. The literature spectra [15] of $MnCr_2O_4$ is also reported. The Mn*K* edge is observed for all the samples at $E = 6544$ eV. This compares well with the value reported in the literature [16] for Mn^{2+}. The maximum at 6547 eV (see dotted line in Fig. 9), that is well evident in BaMn0.5Al11.5 and BaMn1Al11, progressively decreases and reduces to a shoulder of the white peak in the case of BaMn2Al10 and BaMn3Al9. At the same time the position of the white peak gradually shifts towards higher energy (from 6554 to 6557 eV). Both these features suggest that a progressive shift from Mn^{2+} to higher oxidation states occurs on increasing the Mn content. Moreover, the qualitative comparison of the XANES spectra of the Mn-substituted Ba-β-Al_2O_3 samples with those of the reference samples with known Mn valence and location, suggests that Mn is almost entirely present as Mn^{2+} in BaMn0.5Al11.5, while a significant fraction of trivalent and/or tetravalent Mn is present in BaMn2Al10 and BaMn3Al9.

The main results of Rietveld analysis performed on the powder XRD data, collected with both CuK_α and synchrotron radiation, are summarised below. Details on refinement procedures, along with complete refinement results, are reported in a companion paper [17]. The results of Rietveld analysis show that a Ba-β_I-Al_2O_3 phase is formed in all the samples despite amount of Ba higher than stoichiometric, in line with previous literature reports [8]. In the samples with low Mn concentration the refinements indicate the presence of Mn in the tetrahedral Al(2) site (Fig. 10), whereas at higher concentrations, Mn was found also in the octahedral Al(1) sites, while Al(3) and Al(4) do not show any significant evidence of Mn substitution. Mn occupancy in the different Al sites of a semicell is reported in Fig. 11 as a function of the Mn/Ba ratio. At low contents Mn enters only the Al(2) sites with an occupancy that increases almost linearly with Mn loading. For Mn/Ba > 1 the Mn occupancy in the Al(2) site tends to an asymptotic value slightly higher than 0.6, whereas an increasing amount of Mn is found in the Al(1) site. A gradual rise of the occupancy of the Ba sites in the mirror plane for Mn/Ba ratios <1 parallels the increase

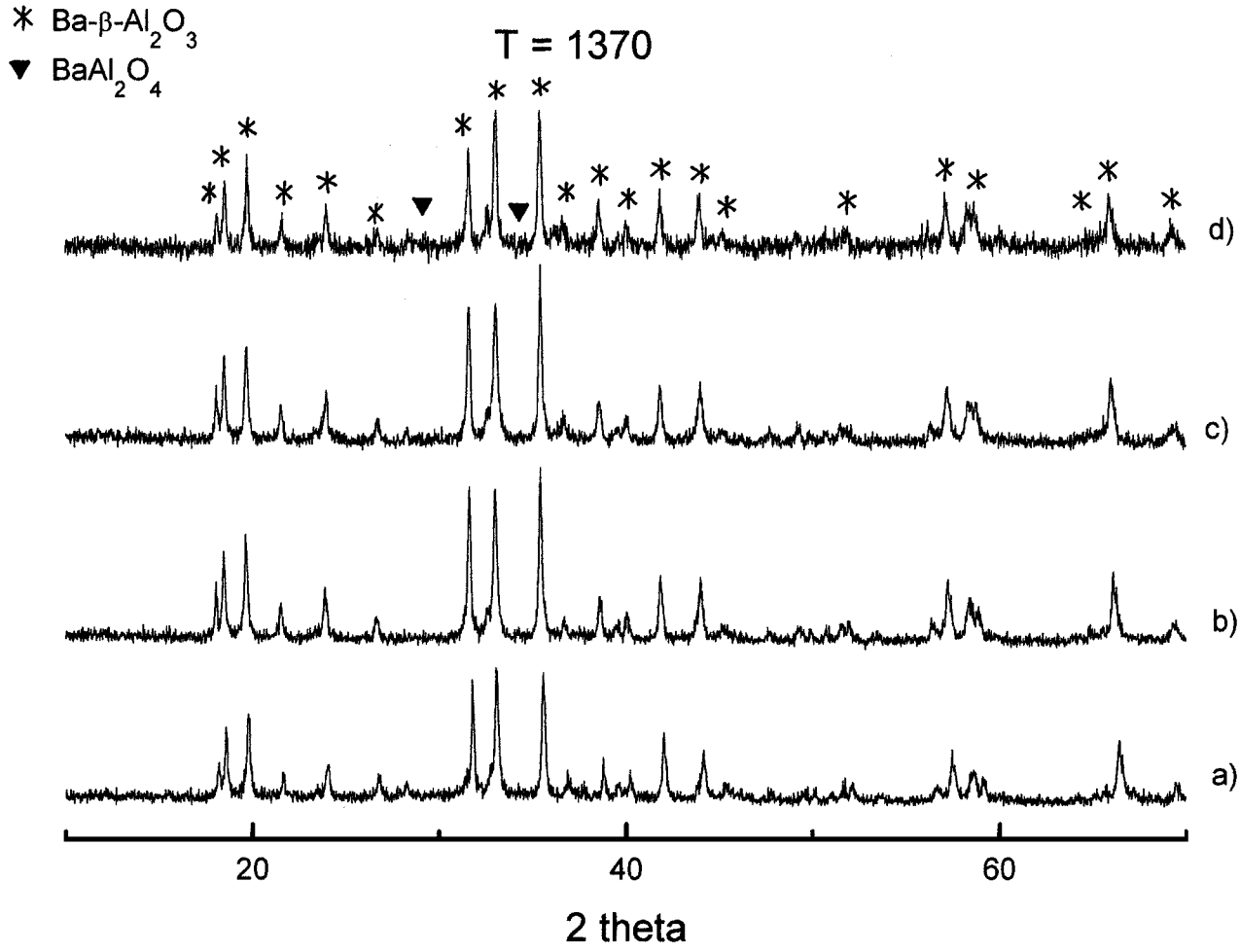

Figure 5 XRD spectra of samples calcined at 1370 K: (a) BaMn0.5Al11.5, (b) BaMn1Al11, (c) BaMn2Al10 and (d) BaMn3Al9.

TABLE I Calculated cell parameters and c_0/a_0 ratio for the different BaMnxAl$(12-x)$

Sample	$a_0 = b_0$ (Å)	c_0 (Å)	c_0/a_0
BaAl12	5.5936(4)	22.767(2)	4.87
BaMn0.5Al11.5	5.6176(3)	22.739(1)	4.05
BaMn1Al11	5.64123(4)	22.7260(3)	4.03
BaMn2Al10	5.65916(3)	22.7529(2)	4.02
BaMn3Al9	5.6719(1)	22.776(1)	4.01

of Mn occupancy in the Al(2) sites. It has to be considered that the presence of one Ba^{2+} ion in the mirror plane instead of one O^{2-} ion (i.e. disappearance of a Reidinger defects) implies a 4+ charge variation. This suggests that a charge compensation mechanism operates to allocate Mn ions in the structure at low Mn/Ba ratio. In fact, the progressive increase of Ba occupancy associated with the decrease of the Reidinger defects can balance the introduction of Mn^{2+} replacing Al^{3+} in the Al(2) sites.

Attribution of dominant II valence for Mn ions in Al(2) sites was also indicated by refined values of the f' anomalous dispersion coefficients that also suggests that Mn in Al(1) sites is mainly trivalent [17].

The calculated cell parameters together with the c_0/a_0 ratios of the different BaMnxAl$(12-x)$ samples are reported in Table I along with those of the unsubstituted $BaAl_{12}O_{13}$ (BaAl12). The smaller values of the a_0 lattice parameter and of the c_0/a_0 ratio vs. Mn loading are in line with the presence of Mn^{2+} in tetrahedral coordination (i.e. Al(2) sites) and with Mn^{3+} in the octahedral one (i.e. Al(1) sites). Indeed, the a_0 lattice parameter increases with the Mn loading in the whole investigated range, even though the rise is steeper up to Mn/Ba = 1 whereas it is less pronounced for higher Mn loading. This behaviour is consistent with the initial substitution of Al(2) with Mn^{2+}, which causes a marked expansion of the site co-ordination distance. Afterwards, substitution of Al(1) with Mn^{3+}, that occurs on increasing further the Mn content, causes only minor site distortions due to close similarity between the ionic radii of Al^{3+} and Mn^{3+}. The trend of the c_0/a_0 ratio is also in line with the above interpretation. At low Mn content the c_0/a_0 ratio decreases almost linearly with the Mn loading. This behaviour agrees quantitatively with that reported in the literature for Mg-doped Ba-β-Al_2O_3 [8] and can be explained as follows: the substitution of Al(2) with divalent Mn reduces the concentration of Ba vacancies and enforces the bonds between the spinel block and the mirror plane, thus the distance between spinel block and the mirror plane is contracted. This compensates for the expansion along the c axis due to incorporation of Mn^{2+} in the spinel block. For Mn/Ba > 1, Mn enters the Al(1) sites mainly as Mn(III) and no further increase of the Ba concentration is observed. Accordingly both c_0 and a_0 expand and their ratio keeps almost constant.

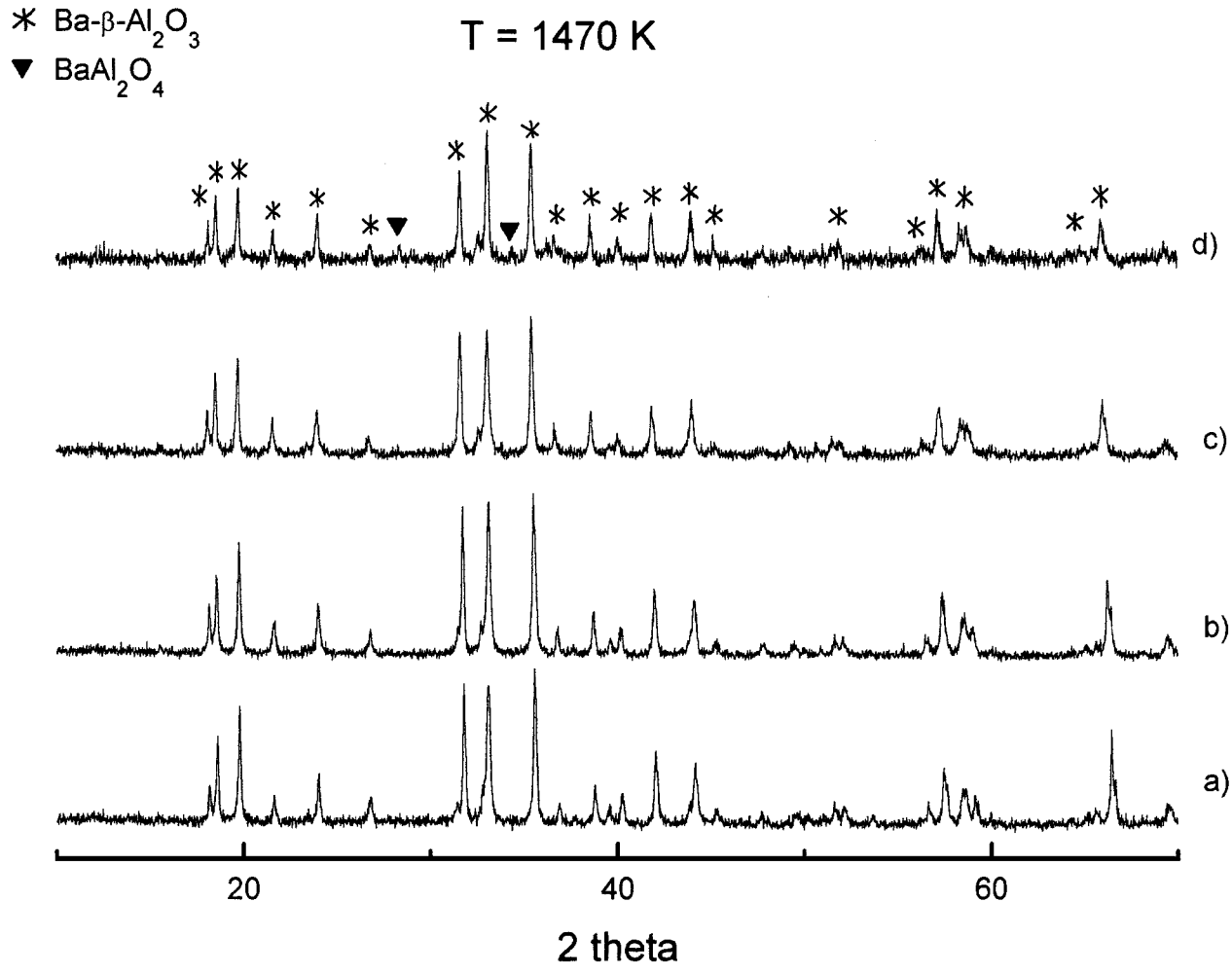

Figure 6 XRD spectra of samples calcined at 1470 K: (a) BaMn0.5Al11.5, (b) BaMn1Al11, (c) BaMn2Al10 and (d) BaMn3Al9.

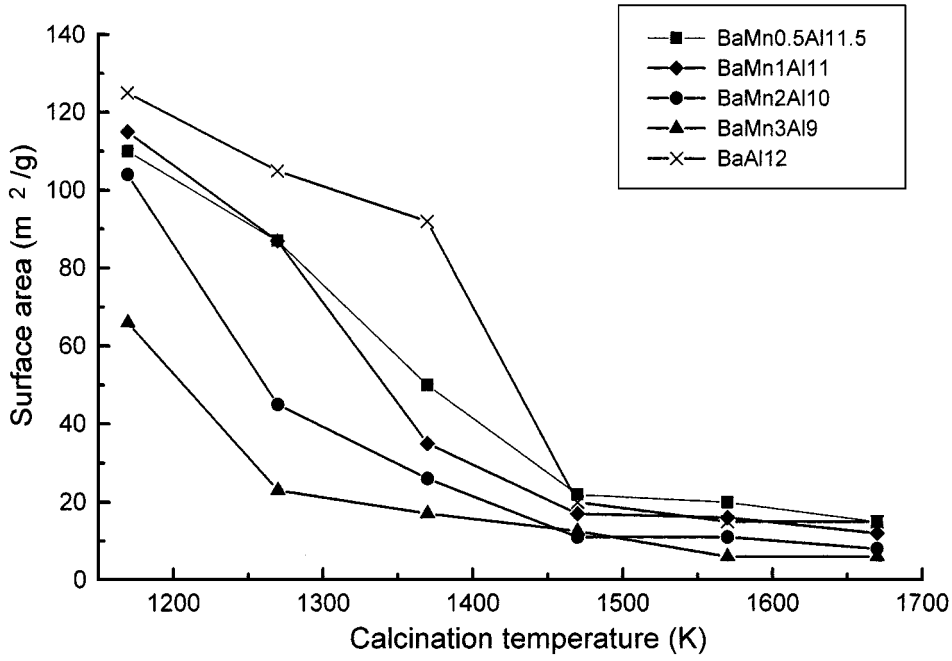

Figure 7 Surface areas of samples calcined in the range 1170–1670.

Structure refinements also allowed for the calculation of the aspect ratios of the anisotropic plate-like crystallites of Ba-β_I-Al_2O_3. In Fig. 12 the calculated values versus the measured BET surface areas are plotted for the Mn-substituted samples and for the unsubstituted $BaAl_{12}O_{19}$ reference sample. Fig. 12 shows that in the Mn-substituted samples both the measured surface area and the calculated aspect ratio decrease with

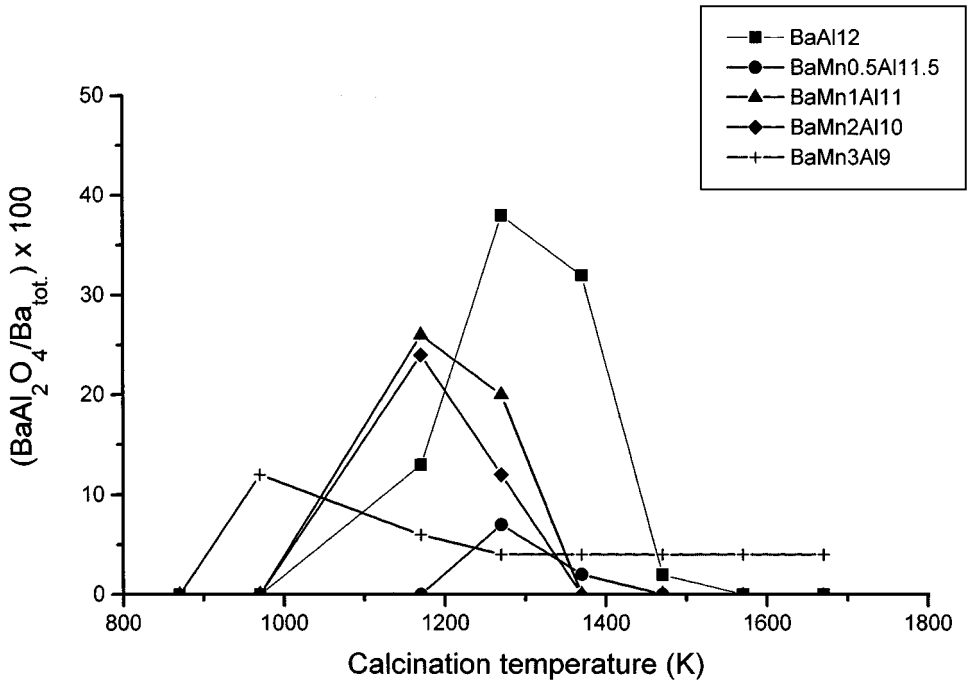

Figure 8 Quantitative XRD analysis of $BaAl_2O_4$.

Mn content. An almost linear correlation is observed that is in line with a report in the literature that the sintering resistance arises from inhibition of the crystal growth along the *c*-axis associated with anisotropic diffusion coefficients [4]. The unsubstituted BaAl12 sample also shows high surface area and large crystallite shape factor but deviates markedly from linear correlation of Mn-substituted materials. This is possibly due to the different microstructure of BaAl12 arising from intergrowth of both β_I-Al_2O_3 and β_{II}-Al_2O_3 domains.

4. Discussion

4.1. Thermal evolution

The phase compositions of the BaMnxAl$(12-x)$ samples calcined at different temperatures are summarised in Table II.

Samples dried at 380 K consist of mixed Ba-Al crystalline compounds and crystalline $MnCO_3$ that easily decompose upon calcination at 770 K to give very microcrystalline materials characterised by high surface areas and high interspersion of the constituents.

Upon calcination at 970 K the crystallisation of α-Mn_2O_3 is detected to an extent that increases with Mn content. However all the samples are essentially microcrystalline in line with the presence of a γ-Al_2O_3 matrix (see XRD base line modulations) that also accounts for the high values of surface area (90–180 m^2/g). At this calcination temperature the incipient formation of $BaAl_2O_4$ is detected only in BaMn3Al9. In all the other samples the formation of $BaAl_2O_4$ is observed starting from 1170 K. For all the Mn-containing materials as well as for BaAl12, the results of quantitative XRD analysis (Fig. 8) shows the presence of a maximum

TABLE II Phase composition of BaMnxAl$(12-x)$ calcined at different temperatures (AACHH = $(NH_4)_2Al_6(OH)_{14}(CO_3)_3{\cdot}H_2O$, Ba-Al = $Ba_2Al_4(OH)_{16}$, $BaAl_2(CO_3)_2(OH)_4{\cdot}2H_2O$).

T_c (K)	BaMn0.5Al11.5	BaMn1Al11	BaMn2Al10	BaMn3Al9
380	AACHH, $MnCO_3$ traces	AACHH, $MnCO_3$, Ba-Al	AACHH, $MnCO_3$, Ba-Al	$MnCO_3$
770	Amorphous	Amorphous	Amorphous	Amorphous
970	α-Mn_2O_3, γ-Al_2O_3	α-Mn_2O_3, γ-Al_2O_3	α-Mn_2O_3, γ-Al_2O_3	α-Mn_2O_3, γ-Al_2O_3, $BaAl_2O_4$
1170	α-Mn_2O_3, γ-Al_2O_3, $BaAl_2O_4$	α-Mn_2O_3, γ-Al_2O_3, $BaAl_2O_4$	α-Mn_2O_3, γ-Al_2O_3, $BaAl_2O_4$	α-Mn_2O_3, γ-Al_2O_3, $BaAl_2O_4$, Ba-β-Al_2O_3
1270	γ-Al_2O_3, $BaAl_2O_4$, Ba-β-Al_2O_3 traces	γ-Al_2O_3, $BaAl_2O_4$, Ba-β-Al_2O_3	γ-Al_2O_3, $BaAl_2O_4$, Ba-β-Al_2O_3	$BaAl_2O_4$, Ba-β-Al_2O_3
1370	$BaAl_2O_4$ traces, Ba-β-Al_2O_3	Ba-β-Al_2O_3	Ba-β-Al_2O_3	$BaAl_2O_4$, Ba-β-Al_2O_3
1470	Ba-β-Al_2O_3	Ba-β-Al_2O_3	Ba-β-Al_2O_3	$BaAl_2O_4$, Ba-β-Al_2O_3
1570	Ba-β-Al_2O_3	Ba-β-Al_2O_3	Ba-β-Al_2O_3	$BaAl_2O_4$, Ba-β-Al_2O_3
1670	Ba-β-Al_2O_3	Ba-β-Al_2O_3	Ba-β-Al_2O_3	$BaAl_2O_4$, Ba-β-Al_2O_3

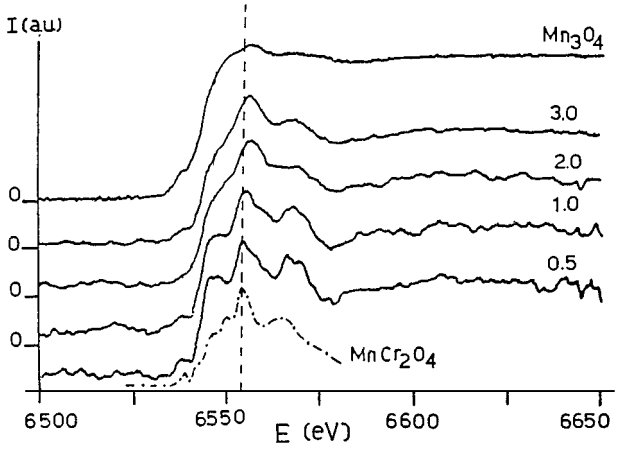

Figure 9 XANES spectra of BaMnxAl$(12-x)$ samples, reference Mn_3O_4, and literature $MnCr_2O_4$.

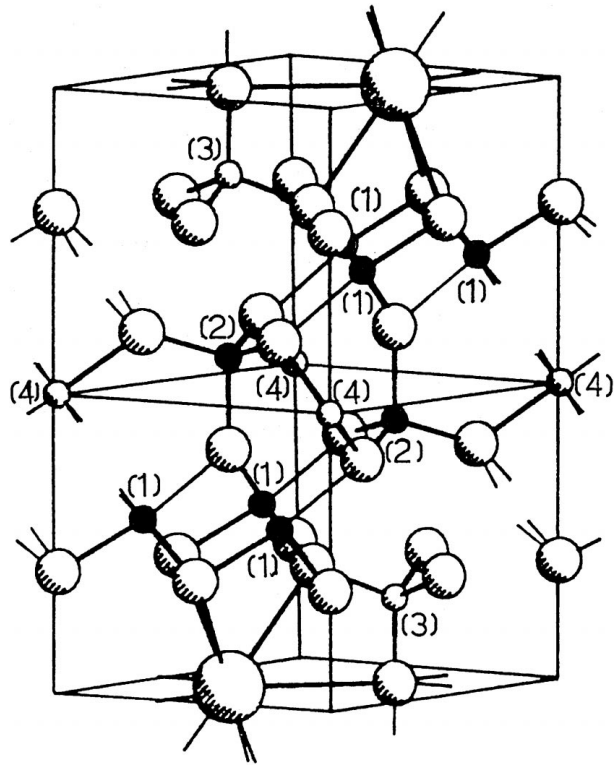

Figure 10 Ideal semicell of Ba-β_I-Al_2O_3. Numbers in parenthesis refer to the different Al sites. Mn positions are indicated by bold spheres.

of $BaAl_2O_4$ concentration. The temperature at which the maximum is observed decreases as the Mn content increases. The decrease of $BaAl_2O_4$ concentration is accompanied by the decrease of α-Mn_2O_3 and by the appearance of the final Ba-β-Al_2O_3 phase. The formation of this latter phase is completed at temperatures that progressively decrease with the Mn content, and is paralleled by the disappearance of $BaAl_2O_4$, except for BaMn3Al9 that segregates small amounts of this phase up to 1670 K. All this suggest that $BaAl_2O_4$ is a reagent in the solid state reaction leading to the formation of the Ba-β-Al_2O_3 .

In a previous study on Mn-free samples (BaAl14, BaAl12, BaAl9) prepared via the same route [4, 10], it was proposed that the formation of the Ba-β-Al_2O_3 phase proceeds through simultaneous solid state reaction between amorphous Ba species and $BaAl_2O_4$ and γ-Al_2O_3. A threshold temperature of 1370 K was found for the formation of the Ba-β-Al_2O_3 phase that was related to the activation of the mobility and diffusion of Ba ions into the γ-Al_2O_3 spinel blocks. The key factor for the achievement of a final monophasic material with high surface area was reported to be the presence of highly interspersed Ba species that hinder alumina transitions up to the formation of the final phase that is favoured by the small dimensions of the aggregates.

The same mechanism can be reasonably hypothesised for the formation of Ba-β_I-Al_2O_3 in Mn-substituted materials. Indeed a similar evolution of phase composition is observed at the intermediate calcination temperatures except in the presence of α-Mn_2O_3. Also in this case the presence of dispersed Ba species can be invoked considering that in all the samples the calculated amount of $BaAl_2O_4$ accounts only for a relatively small fraction of the total Ba content. Such an high interspersion originates from the adopted precipitation conditions. Indeed the dried precursors consist of both very small amorphous aggregates, the presence of which is evidenced by the high specific surface area, and of mixed crystalline phases that easily decompose at low temperature giving rise to amorphous domains where Ba and Al are interspersed at the atomic level.

As with Ba-Al-O systems, in Mn-containing samples, a threshold temperature is observed for the formation of the layered alumina phase that progressively decreases with increasing Mn content. The promoting effect of Mn was related to an increase of ion mobility within the γ-Al_2O_3 spinel blocks that, according to the above mechanism, would be responsible for the easier formation of the final phase. To provide evidence in favour of such increase of ion mobility, the temperatures of phase transition of pure and Mn-doped alumina samples, prepared via coprecipitation, were compared. Indeed, the alumina transitions imply lattice rearrangements that require mobility of oxygen ions. It was shown that the addition of Mn resulted in a lower transition temperature, thus supporting the promoting effect of Mn on ion mobility in the alumina lattice.

4.2. Structural analysis and Mn allocation and oxidation state in the structure

The X-ray powder diffraction spectra of the BaMn0.5Al11.5, BaMn1Al11, BaMn2Al10 samples calcined at 1570 K show the presence of a single Ba-β_I-Al_2O_3 phase only. On the contrary the sample BaMn3Al9 retains a small fraction of $BaAl_2O_4$, that is an intermediate phase in the synthesis of all the samples.

The detailed crystallographic study on Mn-substituted Ba-β-Al_2O_3 reported above shows that, at low concentration, Mn preferentially enters the structure as Mn^{2+} localised in the tetrahedral Al(2) sites. Replacement of Al^{3+} by Mn^{2+} is responsible for a charge compensation mechanism that allows higher Ba occupancy in the mirror plane, thus favouring the formation of Ba-β_I-Al_2O_3 at high Ba/(Al + Mn) ratio. The mechanism of charge compensation also allows for insertion of appreciable amounts of Mn in the Ba-β_I-Al_2O_3 structure without phase segregation. This is not allowed in the

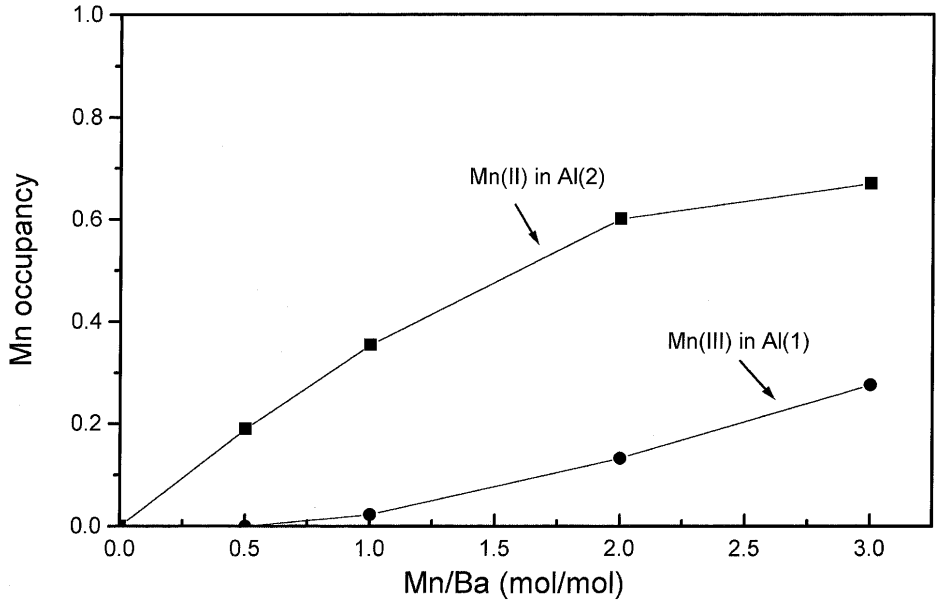

Figure 11 Calculated Mn occupancy in the Al sites of a semicell.

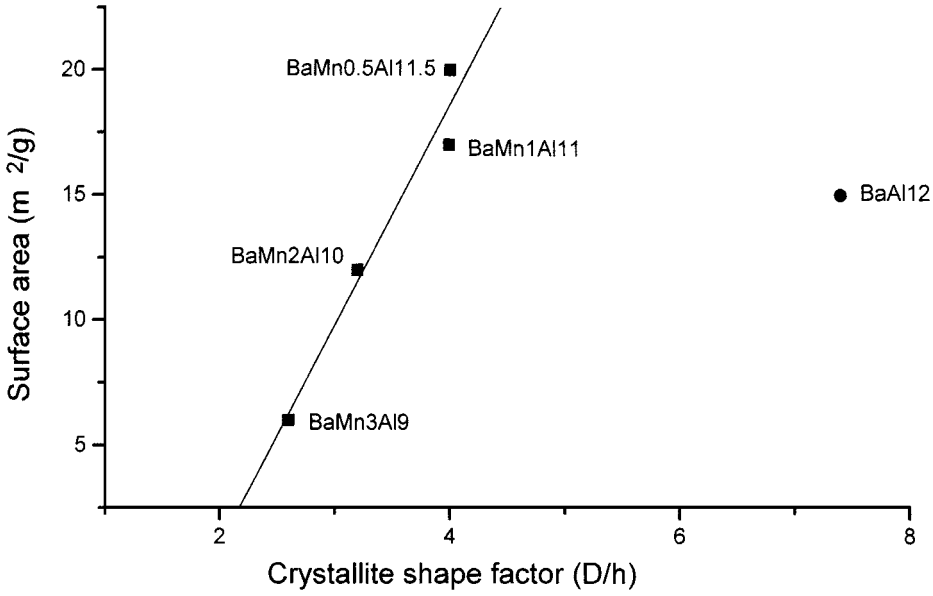

Figure 12 Surface area vs. calculated crystallite shape factors for the different Mn/Ba ratios.

magnetoplumbite structures in which defects of cation vacancies in the mirror planes are not present to any significant extent. Accordingly, elements with higher oxidation states (e.g. Pr^{3+}, La^{3+}) should be inserted in the mirror plane to allow localisation of divalent Mn in the spinel blocks [18].

On increasing the Mn content, Ba sites are progressively saturated. Accordingly, the charge compensation mechanism is no longer allowed and Mn preferentially enters the octahedral Al(1) site as Mn^{3+}. Saturation of Ba sites at high Mn content, might also be responsible for segregation of $BaAl_2O_4$ in the Mn richest sample.

The identification of partitioning and of dominant valence state of Mn in the different crystallographic sites as a function of total Mn loading provides a basis for the discussion of the observed morphological properties. The correlation between surface area and calculated aspect ratio of the crystallites confirms that sintering resistance arises from inhibition of the crystal growth along the c axis due to anisotropic diffusion in the layered structure as already reported for Mn-free systems [4]. The data obtained at low Mn loading (up to Mn/Ba = 1) show that substitution of Al^{3+} with divalent Mn in the Al(2) sites has a minor effect on the morphological properties. On the other hand further Mn insertion in the Al(1) sites with dominant valence 3+ reduces both the surface area and the crystallite aspect ratio. The promoting effect of Mn on high temperature sintering can be related to the increase of ion mobility (Ba^{2+} and O^{2-}) in the spinel blocks that has been held responsible for the formation of the final phase in Mn-containing materials at lower temperatures. The absence of a significant effect on the sintering resistance at low Mn-content could be related to the increase of Ba concentration in the mirror planes associated with substitution of divalent Mn in tetrahedral Al(2). The increase of the sintering resistance on increasing the Ba concentration in the Ba-β-Al_2O_3 structure has been

already reported for Ba-Al-O systems [4, 10] and could balance the Mn effect up to saturation of the Ba sites (i.e. $x = 1.0$).

5. Conclusions

From the present study the following main conclusions can be derived:

1. The preparation route adopted is suitable for obtaining quantitative and reproducible precipitation of the components in precursors that consist of methastable crystalline mixed compounds and an amorphous matrix. Calcination at 770 K of the precursors results in microcrystalline matrixes of high surface areas, in which an high interspersion of the constituents is provided by the starting amorphous precursor and by the decomposition of the original mixed phases. The calcination of these microcrystalline matrixes allows for the achievement of a final material with the Ba-β_I-Al_2O_3 structure. Except for BaMn3Al9, where small amounts of $BaAl_2O_4$ are always detected, monophasic materials with surface areas of 5–15 m^2/g are obtained for all the samples.

2. The formation of the final layered alumina phase occurs at progressively lower temperatures on increasing the Mn content. The promoting effect of Mn is likely associated with the increased ion mobility within the γ-Al_2O_3 spinel blocks that favours the formation of the Ba-β_I-Al_2O_3 via diffusion of Ba ions in the γ-Al_2O_3 matrix.

3. At low concentrations Mn preferentially enters the structure as Mn^{2+} in the tetrahedral Al(2) sites. The resulting charge variation is balanced by the increase of Ba concentration in the mirror planes, this allows for the formation of a β_I-type phase. Beyond saturation of Ba sites corresponding to a Mn occupancy in Al(2) sites of 0.5, this charge compensation mechanism is no longer effective and Mn preferentially enters the structure as Mn^{3+} in octahedral Al(1) sites.

4. At high Mn loading ($x > 2$), Mn promotes high temperature sintering, due to the higher ion mobility in γ-Al_2O_3 spinel blocks induced by Mn. At low Mn loading such an effect is balanced by the increase of Ba occupancy in the mirror planes.

Acknowledgements

Financial support for this work has been provided by MURST, Roma, Italy. Access to the SRS beam station was made possible by the EC Large Installation Plan. Thanks are due to Prof. G. Artioli of Universitá degli Studi di Milano for stimulating discussion and criticism.

References

1. M. F. M. ZWINKELS, S. G. JÄRÅS, P. G. MENON, and T. GRIFFIN, *Catal. Rev. -Sci. Eng.* **35** (1993) 319.
2. G. GROPPI, C. CRISTIANI and P. FORZATTI, *Catalysis* **13** (1997) 85.
3. M. MACHIDA, A. SATO, T. KIJIMA, H. INOUE, K. EGUCHI and H. ARAI, *Catalysis Today* **26** (1995) 239.
4. G. GROPPI, F. ASSANDRI, M. BELLOTTO, C. CRISTIANI and P. FORZATTI, *J. Solid State Chem.* **114** (1995) 326.
5. N. IYI, Z. INOUE, S. TAKEKAWA and S. KIMURA, *ibid.* **52** (1984) 66.
6. *Idem., ibid.* **60** (1985) 41.
7. M. MACHIDA, K. EGUCHI and H. ARAI, *J. Catal.* **123** (1990) 477.
8. B. M. J. SMETS and J. G. VERLIJSDONK, *Mater. Res. Bull.* **21** (1986) 1305.
9. R. C. BARKLIE and K. O'DONNELL, *J. Phys. C: Solid State Phys.* **10** (1977) 4127.
10. G. GROPPI, C. CRISTIANI, P. FORZATTI and M. BELLOTTO, *J. Mater. Sci.* **29** (1994) 3441.
11. G. GROPPI, M. BELLOTTO, C. CRISTIANI, P. FORZATTI and P. L. VILLA, *Appl. Catal. A: General* **104** (1993) 101.
12. H. P. KLUG and L. E. ALEXANDER, "X-Ray Diffraction Procedures" (Wiley, New York, 1974).
13. A. C. LARSON and R. B. VON DREELE, Document LAUR 86-748, Los Alamos Laboratory, 1995.
14. R. F. VOGEL, G. MARCELIN and W. L. KHEL, *Appl. Catal.* **12** (1984) 237.
15. A. MANCEAU, A. I. GORSHKOV and V. A. DRITS, *Amer. Mineral.* **77** (1992) 1133.
16. S. C. KOHN, J. M. CHARNOCK, C. M. B. HENDERSON and G. N. GREAVES, *Contrib. Mineral. Petrol.* **105** (1990) 359.
17. M. BELLOTTO, G. ARTIOLI, C. CRISTIANI, P. FORZATTI and G. GROPPI, *J. Catal.* **179** (1998) 597.
18. K. EGUCHI, H. INOUE, K. SEKIZAWA and H. ARAI, *Studies in Surface Science and Catalysis* **101** (1996) 417.

Received 29 January
and accepted 15 December 1998